

Numerical Simulation of Coextrusion and Film Casting

FORTIN A., CARRIER P.,

*Département de Mathématiques Appliquées,
École Polytechnique de Montréal,
C.P.6079, Succursale Centre-Ville,
Montréal, Canada, H3C 3A7*

and

DEMAY Y.,

*Institut non-linéaire de Nice,
1361 Route des Lucioles,
Sophia-Antipolis,
06560 Valbonne, France*

February 12, 1997

Summary

In the first part of this paper, a numerical strategy is developed for the numerical simulation of the coextrusion process. Coextrusion consists in extruding many polymers in the same die in order to combine their respective properties. The die is generally flat and quite large and consequently, a two-dimensional approximation is sufficient. The main difficulty is to accurately predict the interfaces between the different layers of polymers. A

finite element method based on a pseudo-concentration function is developed to calculate these fluid interfaces. Numerical results are presented for the coextrusion of up to five fluids.

In the second part of the paper, the above strategy is slightly modified to simulate the film casting process. In this case, a polymer is stretched (with a draw velocity U_L) at the exit of the die in order to produce a very thin layer of polymer that is cooled in contact with a chill roll. Only one polymer-air interface has to be computed. The draw ratio is defined as

$$Dr = \frac{U_L}{\bar{U}}$$

where \bar{U} is the mean velocity of the polymer at the exit of the die. As the draw ratio is increased, instabilities appear and numerical results put in evidence the draw resonance phenomenon.

1 Introduction

Polymers are omnipresent. They are used in the aerospace industry, in automobiles and in a large amount of everyday objects. Many processes exist in the polymer industry. One of them is the coextrusion process which is particularly important in the wrapping industry. The idea is to combine many non-miscible polymers to obtain a product with specific properties such as impermeability, esthetic quality, resistance, etc. In that specific case, the molten polymers are extruded in a flat die. The main difficulty of this process is to balance the flow in order to obtain optimal thicknesses for each layer of polymer. These thicknesses will strongly depend on the shear-thinning behaviour of the polymers and on the different flowrates imposed at the inlet of the die (see Agassant-Fortin- Demay [2]).

To compute fluid interfaces, at least two strategies are possible: tracking and capturing. The first strategy tracks the interface and requires full or partial remeshing of the domain in order to follow the interfaces. Consequently, the mesh evolves until it matches the different interfaces. The reader is referred to Crochet [7] for an application of the tracking method to the numerical prediction of extrudate swell. This method requires very efficient remeshing techniques and does not seem to be well adapted for time-dependent problems.

On the other hand, the capturing strategy requires a single mesh and the different interfaces are determined by a function S (often called the pseudo-concentration) which is computed in the whole domain. This however requires the solution of a supplementary partial differential equation of hyperbolic type of the form

$$\frac{\partial}{\partial t}S(\vec{x}, t) + (\vec{u} \cdot \vec{\nabla})S(\vec{x}, t) = 0, \quad \forall \vec{x} \in \Omega.$$

where $\vec{u} = (u_1(\vec{x}), u_2(\vec{x}))$ is the velocity field. This strategy was adopted in the Volume of Fluid (VOF) method of Hirt and Nichols [17] and in the pseudo-concentration method of Thompson [24]. The reader is referred to the excellent paper of Shen [23] for a review of these methods in the context of injection moulding.

In this paper, a capturing strategy is adopted since we are interested in both stationary and time-dependent problems (see Agassant-Fortin-Demay [2], Carrier [6], Fortin-Demay-Agassant [10]). The discontinuous Galerkin method is used for the computation of the pseudo-concentration function. Numerical results shows the accuracy and flexibility of the proposed method.

Let us now present the equations governing the movement of the polymer and the interface positions.

2 Equations

2.1 Stokes Problem

In these simulations, inertia and gravitational forces are neglected as it is the case for most polymer processing applications (see [1]). Moreover, surface tension is not taken into account at fluid interfaces since it is generally negligible in the two applications under study. Consequently, the momentum equations can be written as

$$\vec{\nabla} \cdot \boldsymbol{\sigma} = 0, \tag{1}$$

where $\boldsymbol{\sigma}$ is the Cauchy stress tensor defined by

$$\boldsymbol{\sigma} = -p\mathbf{I} + \boldsymbol{\tau}. \tag{2}$$

The extra-stress tensor $\boldsymbol{\tau}$ is related to the velocity field by the relation (see Bird et al. [4]):

$$\boldsymbol{\tau} = 2\eta(|\dot{\boldsymbol{\gamma}}|)\dot{\boldsymbol{\gamma}}(\vec{u}) \tag{3}$$

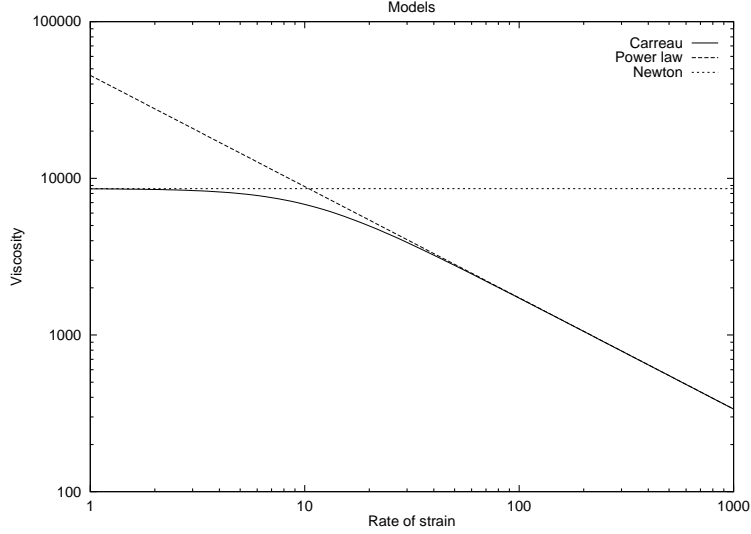


Figure 1: *Viscosity models*

where $\dot{\gamma}(\vec{u}) = 1/2[\vec{\nabla}\vec{u} + (\vec{\nabla}\vec{u})^t]$ is the rate of deformation tensor and $|\dot{\gamma}| = \sqrt{\dot{\gamma}_{ij}\dot{\gamma}_{ji}}$, its norm (the Einstein notation has been used). One can remark that the viscosity η depends on the norm of the rate of deformation tensor $|\dot{\gamma}|$, expressing the shear-thinning behaviour of polymers.

Different models exist, all based on experimental data, to take into account shear-thinning effects. Figure 1 illustrates three of these models: the Newtonian law, the power law and the Carreau model. The last one is the most general because it follows experimental data on a wider range of rate of deformation. The viscosity law has the following form:

$$\eta(|\dot{\gamma}|) = \eta_0(c + \lambda^2|\dot{\gamma}|^2)^{\frac{n-1}{2}} \quad (4)$$

where the Carreau law corresponds to $c = 1$. Usually, λ , η_0 and n are determined from experimental data through curve fitting. The power law is obtained by setting $c = 0$ while the Newtonian law corresponds to $n = 1$ (constant viscosity).

Finally, combining all these properties, the problem to solve becomes

$$2\vec{\nabla} \cdot [\eta(|\dot{\gamma}|)\dot{\gamma}(\vec{u})] = \vec{\nabla}p \quad (5)$$

together with the incompressibility condition:

$$\vec{\nabla} \cdot \vec{u} = 0 \quad (6)$$

Finally, a supplementary equation is needed to determine the position of the interface between any two molten polymers. This position is determined by a transport equation described in the next section.

2.2 The pseudo-concentration method

For the sake of completeness, let us recall the basic assumptions of the pseudo-concentration method introduced by Thompson ([24] [25]) and which presents similarities with the Volume of Fluid method of Hirt and Nichols [17].

At polymer interfaces, two conditions are to be satisfied. The first one merely states that the interface is at equilibrium and can be written as

$$\boldsymbol{\sigma}_1 \cdot \vec{n} = \boldsymbol{\sigma}_2 \cdot \vec{n}, \quad (7)$$

where $\boldsymbol{\sigma}_i, i = 1, 2$ is the Cauchy stress tensor on each side of the interface and \vec{n} is the normal vector. This condition will be a direct consequence of the variational formulation as will be discussed in section 3.

The second condition on the interface expresses the non-miscibility of the polymers. Suppose that two polymers are coextruded. The general case is similar. They are separated by the interface \mathcal{H} which is *a priori* unknown. Figure 2 illustrates the domain. One can define a fonction $S(\vec{x}, t)$ in the

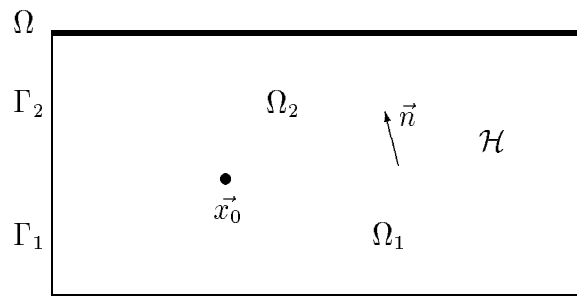


Figure 2: *Domain with two fluids*

whole domain Ω by setting

$$S(\vec{x}, t) = \begin{cases} 1 & \text{if } \vec{x} \in \Omega_1 \\ 0 & \text{if } \vec{x} \in \Omega_2. \end{cases} \quad (8)$$

This function is called the pseudo-concentration. The position of the interface is at the jump of the function S (see Figure 2).

To compute the pseudo-concentration, let us consider an initial volume \mathcal{V}_0 in Ω containing the same particles at any time. At time t , the volume \mathcal{V}_0 is allowed to deform with the flow and to become \mathcal{V}_t . Any particule inside \mathcal{V}_0 at $t = 0$ will remain in \mathcal{V}_t at time t . Consequently,

$$\frac{d}{dt} \int_{\mathcal{V}_t} S(\vec{x}, t) dx dy = 0 \quad (9)$$

One can show (see Ottino [20]) that,

$$\frac{d}{dt} \int_{\mathcal{V}_t} S(\vec{x}, t) dx dy = \int_{\mathcal{V}_t} \frac{D}{Dt} S(\vec{x}, t) dx dy \quad (10)$$

where $\frac{D}{Dt} = \frac{\partial}{\partial t} + (\vec{u} \cdot \vec{\nabla})$. Since this is true for all \mathcal{V}_0 (and thus for all \mathcal{V}_t), we get the condition

$$\frac{\partial}{\partial t} S(\vec{x}, t) + (\vec{u} \cdot \vec{\nabla}) S(\vec{x}, t) = 0, \quad \forall \vec{x} \in \Omega. \quad (11)$$

This relation is valid in the entire domain Ω . In other words, the solution of this transport equation (12) is equivalent to the non-miscibility condition and also determines the position of the interface between the two fluids. This is done by searching the jump in the function S . On a practical standpoint, one looks for the isovalue 1/2 of the function S .

For the coextrusion problem, stationary solutions only are of interest and the time derivative term is neglected. The equation reduces to

$$(\vec{u} \cdot \vec{\nabla}) S(\vec{x}) = 0, \quad \forall \vec{x} \in \Omega. \quad (12)$$

However, for film casting problems, (see Barq [3], Demay-Agassant [8]) time-dependent solutions arise after the onset of the instabilities and in that case,

the time derivative will be discretized by a fully implicit Gear Scheme which can be written as

$$\frac{\partial S(\vec{x}, t_{n+1})}{\partial t} \simeq \frac{3S(\vec{x}, t_{n+1}) - 4S(\vec{x}, t_n) + S(\vec{x}, t_{n-1})}{2\Delta t}, \quad (13)$$

The Gear scheme is second order in time and was proven to be very accurate for the prediction of time-dependent problems (see Fortin-Fortin-Gervais [12]).

2.3 Boundary Conditions

Suppose p fluids are coextruded in a very simple flat die like the one in figure 3. Then $\Omega = \bigcup_{k=1}^p \Omega_k$. The interfaces are between each domain Ω_k , $k =$

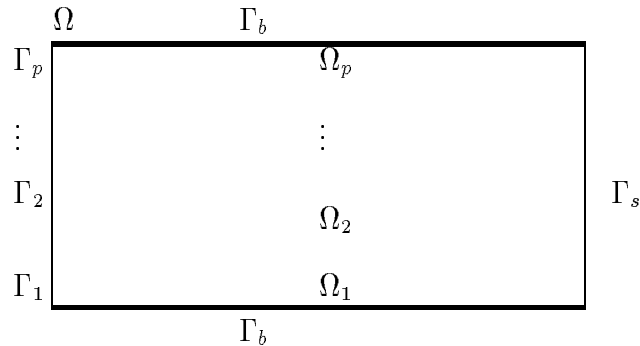


Figure 3: *Boundary conditions for coextrusion*

$1, \dots, p - 1$ and their positions are *a priori* unknown.

Boundary conditions for the velocity field must be provided on each of the Γ_k . This is a delicate question since the flow can be rather complex before entering the die. However, since viscoelastic effects are neglected, the developed velocity profile in the die should not depend on the precise form of the imposed velocity profile on Γ_k . The interfaces depend strongly however, on the respective flowrates Q^k in each layer of polymer. Consequently, parabolic profiles with given flowrates Q^k are imposed on each Γ_k . Flat profiles with the same flowrates would give similar results.

A no-slip condition is imposed on each plate Γ_b on top and bottom of the die. At the die exit, the flow, and thus the interfaces, is supposed fully developed.

To summarize, the boundary conditions are:

$$\begin{aligned} \vec{u}^k &= Q^k(u_0^k(y), 0) & \vec{x} \in \Gamma_k & \quad k = 1, \dots, p \\ \vec{u} &= 0 & \vec{x} \in \Gamma_b & \\ u_2 = 0 & \quad , \quad (\boldsymbol{\sigma} \cdot \vec{n})_x = 0 & \vec{x} \in \Gamma_s & \end{aligned} \quad (14)$$

where $u_0^k(y)$ are parabolic profiles with unit flowrate. In this manner, the flowrates in each layer can be easily changed and their effects on the interfaces can be put in evidence.

For the transport equation (12), a boundary condition must be provided only on the inflow part of the boundary defined as:

$$\partial\Omega^- = \{\vec{x} \in \Omega \mid \vec{u}(\vec{x}) \cdot \vec{n}(\vec{x}) < 0\}. \quad (15)$$

The inflow boundary value of S will be transported in all the domain by the velocity field \vec{u} . The different fluids are distinguished by setting S to different values on $\Gamma_1, \dots, \Gamma_p$ (thus the name pseudo-concentration). The following choice was used:

$$S^k = \frac{p-k}{p-1}, \quad \vec{x} \in \Gamma_k, \quad k = 1, \dots, p, \quad (16)$$

with $p \geq 2$. The different jumps in the step function (16) will give the position of the interfaces.

Finally, the equilibrium of the interface

$$\boldsymbol{\sigma}^k \cdot \vec{n} = \boldsymbol{\sigma}^{k+1} \cdot \vec{n}, \quad \vec{x} \in \mathcal{H}^k, \quad k = 1, \dots, p-1. \quad (17)$$

is automatically satisfied by the variational formulation as we shall see in section 3.

3 Variational Formulations

Appropriate variational formulations are needed for both the generalized Stokes problem and the transport equation for the pseudo- concentration.

$$\left\{ \begin{array}{l} 2\vec{\nabla} \cdot [\eta(|\dot{\gamma}|)\dot{\gamma}(\vec{u})] = \vec{\nabla}p \\ \vec{\nabla} \cdot \vec{u} = 0 \\ (u \cdot \vec{\nabla})S = 0 \end{array} \right. \quad (18)$$

System (18) is a coupled problem for the three unknowns (\vec{u}, p, S) . To avoid the assembly and factorization of a huge matrix, and to take advantage of the discontinuous Galerkin method which allows the solution of the transport equation on an element by element basis, a Picard type iterative scheme will be used to solve this system. Variational formulations are then needed for both the generalized Stokes problem and the transport equation.

3.1 The generalized Stokes Problem

Let us suppose at this time that S is known (from a previous iteration for example). From the value of S , it is possible to determine the domain Ω_k where is located the k^{th} fluid.

The boundary of Ω is separated into two parts corresponding to essential (Γ_{ess}) and natural (Γ_{nat}) boundary conditions. Thus, $\Gamma = \Gamma_{ess} \cup \Gamma_{nat}$ and we take $\vec{v} \in H_{\Gamma_{ess}}^1(\Omega)^2$ defined by

$$\begin{aligned} H_{\Gamma_{ess}}^1(\Omega)^2 &= \{ \vec{v} \in H^1(\Omega)^2 \mid \vec{v} = \vec{0} \text{ on } \Gamma_{ess} \} \\ H^1(\Omega)^2 &= \{ \vec{v} \in \mathcal{L}^2(\Omega)^2 \mid \int_{\Omega} \vec{\nabla} \vec{v} : \vec{\nabla} \vec{v} < \infty \} \\ \mathcal{L}^2(\Omega) &= \{ q \mid \int_{\Omega} q \cdot q < \infty \}. \end{aligned}$$

The momentum equation is then multiplied by $\vec{v} \in H_{\Gamma_{ess}}^1(\Omega)^2$ and integrated by parts while the incompressibility condition is multiplied by $q \in \mathcal{L}^2(\Omega)$ and integrated over the domain. This yields the following variational formulation

for the generalized Stokes problem:

$$\begin{cases} \sum_{k=1}^p \left[\int_{\Omega_k} 2\eta_k(|\dot{\gamma}|)(\dot{\gamma}(\vec{u}) : \dot{\gamma}(\vec{v})) d\Omega - \int_{\Gamma_{\text{nat}}} (\boldsymbol{\sigma}_k \cdot \vec{n}) \cdot \vec{v} d\Gamma \right. \\ \left. - \int_{\Omega_k} (\vec{\nabla} \cdot \vec{v}) p_k d\Omega \right] = 0, & \forall \vec{v} \in H_{\Gamma_{\text{ess}}}^1(\Omega)^2 \\ \int_{\Omega} (\vec{\nabla} \cdot \vec{u}) q d\Omega = 0, & \forall q \in \mathcal{L}^2(\Omega), \end{cases} \quad (19)$$

with the viscosity model for the k^{th} fluid given by:

$$\eta_k(|\dot{\gamma}|) = \eta_0^k (c_k + \lambda_k^2 |\dot{\gamma}|^2)^{\frac{n_k-1}{2}}. \quad (20)$$

3.1.1 Equilibrium of the interfaces

As already mentioned, the equilibrium condition $\boldsymbol{\sigma}^k \cdot \vec{n} = \boldsymbol{\sigma}^{k+1} \cdot \vec{n}$ is natural with this formulation. Indeed, let us consider the domain of figure 2. Taking successively $\vec{v} \in \mathcal{D}(\Omega_1)$ and $\vec{v} \in \mathcal{D}(\Omega_2)$ where $\Omega = \Omega_1 \cup \Omega_2$ and where $\mathcal{D}(\Omega_i)$, $i = 1, 2$ is the space of infinitely differentiable functions with compact support. Integrating by parts on Ω_1 and on Ω_2 separately, we get the formulations

$$- \int_{\Omega_i} \vec{\nabla} \cdot [2\eta_i(|\dot{\gamma}|)\dot{\gamma}(\vec{u})] \cdot \vec{v} d\Omega + \int_{\Omega_i} \vec{\nabla} p_i \cdot \vec{v} d\Omega = 0, \quad i = 1, 2 \quad (21)$$

which means that the momentum equations are satisfied in the distribution sense in each domain Ω_i , $i = 1, 2$. Taking now $\vec{v} \in H_{\Gamma_{\text{ess}}}^1(\Omega)^2$ and integrating by parts with \vec{n} fixed arbitrarily as pointing outward Ω_1 , thus $\vec{n} = \vec{n}_1 = -\vec{n}_2$, we get:

$$\begin{aligned} \sum_{i=1}^2 \left[- \int_{\Omega_i} \vec{\nabla} \cdot 2\eta_i(|\dot{\gamma}|)\dot{\gamma}(\vec{u}) \cdot \vec{v} d\Omega + \int_{\Omega_i} (\vec{\nabla} p_i \cdot \vec{v}) d\Omega \right] \\ + \int_{\mathcal{H}} 2(\eta_1(|\dot{\gamma}|) - \eta_2(|\dot{\gamma}|)) \dot{\gamma}(\vec{u}) \cdot \vec{n} \cdot \vec{v} dS \\ - \int_{\mathcal{H}} ((p_1 - p_2)\mathbf{I} \cdot \vec{n}) \cdot \vec{v} dS = 0. \end{aligned} \quad (22)$$

The first two terms in the sommation vanish since the momentum equation is satisfied in each domain. Using the definition of equation of $\boldsymbol{\sigma}$ (see (2)), we get:

$$\int_{\mathcal{H}} [(\boldsymbol{\sigma}^1 - \boldsymbol{\sigma}^2) \cdot \vec{n}] \cdot \vec{v} d\Omega = 0, \quad \forall \vec{v} \in H_{\Gamma_{\text{ess}}}^1(\Omega)^2. \quad (23)$$

which is equivalent to

$$\boldsymbol{\sigma}_1 \cdot \vec{n} = \boldsymbol{\sigma}_2 \cdot \vec{n}, \quad \forall \vec{x} \in \mathcal{H}. \quad (24)$$

3.1.2 Linearization of the Stokes Problem

The variational formulation (19) is non-linear due the viscosity model. Moreover, it is constrained by the incompressibility condition. A combination of the Newton-Raphson method and of the Uzawa's algorithm was used to solve Stokes type problems as described in [14] and [16]. The Newton-Raphson method takes care of the non-linearities and the Uzawa's algorithm enforces the incompressibility condition. It gives the following algorithm:

$$\begin{aligned} & (\vec{u}_0, p_0) \text{ given,} \\ & \text{For } l \geq 0, \text{ solve} \\ & \left\{ \begin{array}{l} \int_{\Omega} 2\eta_0 (c + \lambda^2 |\dot{\gamma}(\vec{u}_l)|^2)^{\frac{n-1}{2}} (\dot{\gamma}(\delta \vec{u}_l) : \dot{\gamma}(\vec{v})) d\Omega + \\ 2(n-1)\eta_0 \int_{\Omega} (c + \lambda^2 |\dot{\gamma}(\vec{u}_l)|^2)^{\frac{n-3}{2}} (\dot{\gamma}(\vec{u}_l) : \dot{\gamma}(\delta \vec{u}_l)) (\dot{\gamma}(\vec{u}_l) : \dot{\gamma}(\vec{v})) d\Omega \\ + r \int_{\Omega} (\vec{\nabla} \cdot \delta \vec{u}_l) (\vec{\nabla} \cdot \vec{v}) d\Omega = F(\vec{u}_l, p_l) + r \int_{\Omega} (\vec{\nabla} \cdot \vec{u}_l) (\vec{\nabla} \cdot \vec{v}) d\Omega \\ \vec{u}_{l+1} = \vec{u}_l - \delta \vec{u}_l \\ p_{l+1} = p_l - r \vec{\nabla} \cdot \vec{u}_{l+1} \\ \text{if } |\delta \vec{u}_l| < \epsilon, \text{ and } |\vec{\nabla} \cdot \vec{u}_{l+1}| < \epsilon \text{ stop.} \end{array} \right. \quad (25) \end{aligned}$$

where F is the residual defined by:

$$\begin{aligned} F(\vec{u}_l, p_l) &= 2 \int_{\Omega} \eta(|\dot{\gamma}(\vec{u}_l)|) (\dot{\gamma}(\vec{u}_l) : \dot{\gamma}(\vec{v})) d\Omega \\ &\quad - \int_{\Gamma_{\text{nat}}} (\boldsymbol{\sigma} \cdot \vec{n}) \cdot \vec{v} dS - \int_{\Omega} (\vec{\nabla} \cdot \vec{v}) p_l d\Omega, \quad (26) \end{aligned}$$

r is a penalization parameter and $:$ stands for the double contraction product of two tensors.

In the variational formulation (25), we have not indicated the different domain Ω_k for simplicity. In fact, the rheological parameters c , λ and n are functions of the pseudo- concentration S . Since S is known, when computing the elementary matrices, the value of S is evaluated at each Gauss point and its value identifies the polymer. The viscosity coefficients takes then the value of the corresponding polymer.

3.2 The Transport Equation

A variational formulation is also required for the transport equation (12). We now thus suppose that \vec{u} is given.

The solution of the transport equation needs to be very accurate since it determines the position of the interfaces. Transport equations are particularly difficult to solve when discontinuous solutions are present. This is the reason why it is suggested to transport smooth pseudo-concentration functions in order to avoid numerical oscillations (see [24], [9]). We believe that it possible to transport a discontinuous pseudo-concentration, provided the discontinuous Galerkin method is used to solve (12). (see [10],[18] and [21]). As discussed in Johnson [18], the discontinuous Galerkin method is among the best in that case. Very sharp discontinuous solutions can be computed, at the price of very small amplitude wiggles in the vicinity of the discontinuities. These wiggles do not prevent accurate prediction of interfaces and do not generate numerical instabilities.

One of the main features of this method is that it allows the solution of (12) on an element by element basis. Indeed, since S is discontinuous, it seems natural to use discontinuous approximations and to define

$$V_h = \{w \mid w|_K \in P_k(K), \forall K \in \mathcal{T}_n\}, \quad (27)$$

where K is an element of the triangulation and $P_k(K)$ the set of polynomials of degree k on the element K . It is important to remark that no continuity is required at element interfaces. This choice is partly motivated by the fact that the solution S is inevitably discontinuous and has the form

$$S = \begin{cases} 1 & \text{if } \vec{x} \in \Omega_1 \\ 0 & \text{if } \vec{x} \in \Omega_2. \end{cases} \quad (28)$$

The discontinuous Galerkin method ([18]) takes the following form. On each element K , solve

$$\int_K \vec{u} \cdot \vec{\nabla} S \omega d\Omega - \int_{\partial K^-} S(\vec{u} \cdot \vec{n}) \omega dS = - \int_{\partial K^-} S^-(\vec{u} \cdot \vec{n}) \omega dS \quad \forall \omega \in P_k(K), \quad (29)$$

Referring to Figure 4, since the approximation is discontinuous at element interfaces, S^- is the value of S in the element adjacent to K on the inflow part ∂K^- of the boundary of the element K . More precisely, let us define

$$\partial K^- = \{\vec{x} \in \partial K \mid \vec{u}(\vec{x}) \cdot \vec{n}(\vec{x}) < 0\}, \quad (30)$$

$$S = \lim_{\epsilon \rightarrow 0} S(\vec{x} + \epsilon \vec{u}), \quad (\vec{x} \in \partial K^-), \quad (31)$$

and

$$S^- = \lim_{\epsilon \rightarrow 0} S(\vec{x} - \epsilon \vec{u}), \quad (\vec{x} \in \partial K^-). \quad (32)$$

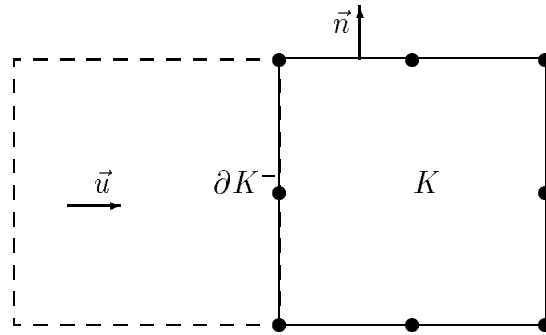


Figure 4: *Two adjacent elements*

An important feature of the discontinuous Galerkin method is that equation (29) results in a small linear system on each element. It can be easily solved on element K but only if S^- has already been computed. This implies that the elements must be solved in a proper order. Such an order usually exists (see [21]) when there is no recirculation zones. The idea is to start with elements adjacent to $\partial\Omega^-$ and to follow the flowfield \vec{u} . A good numbering of the elements (in accordance to the flow) accelerates the convergence but it is not essential for convergence. If the numbering is not optimal or if there exists a recirculation zone in the flowfield, the elements can be swept many times until convergence. The discontinuous Galerkin method is then a block Gauss-Seidel method.

4 Algorithms

In this case, the Picard algorithm becomes:

1. For a given value of S , the rheological constants in the Carreau model can be deduced at each Gauss point and the Stokes problem (5)-(6) is solved with the algorithm (25).
2. For a given value of \vec{u} , the transport equation (12) is solved using the algorithm (29) to get a new value of S noted S^{new}
3. If $\|S - S^{new}\| < \epsilon$, STOP, else $S = S^{new}$ and go to step 1.

4.1 Discretization

The three variables to discretize are the velocity \vec{u} , the pressure p and the pseudo-concentration S . For the velocity and pressure, the $\mathbf{Q}_2^9 - \mathbf{P}_1$ quadratic element was used. Figure 5 illustrates these elements. This ele-

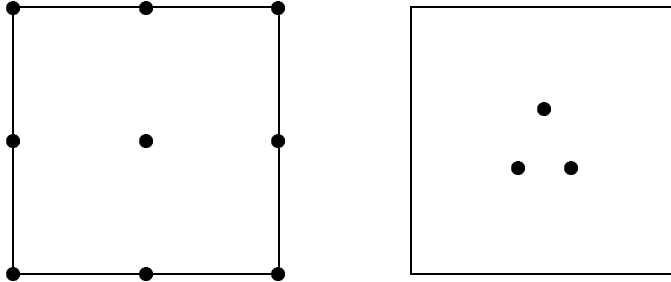


Figure 5: $\mathbf{Q}_2^9 - \mathbf{P}_1$ element

ment satisfies the **Ladyzenskaya-Babuška-Brezzi (L.B.B)** condition (see Brezzi-Fortin [5],[15]) and is one of the best two-dimensional elements..

For the pseudo-concentration function S , the \mathbf{Q}_2^8 element depicted in Figure 6 was chosen. A \mathbf{Q}_1 approximation can also be used but the quadratic element provided the best results. This choice was motivated by our experience with viscoelastic fluid flow problems where a transport equation has to be solved for the stresses. A LBB condition also exists in that case which is satisfied by the above discretizations (see Fortin-Zine-Agassant [13]).

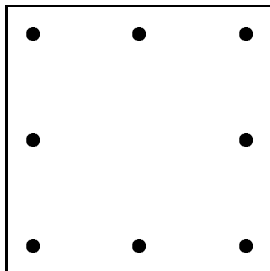


Figure 6: The Q_2^8 element

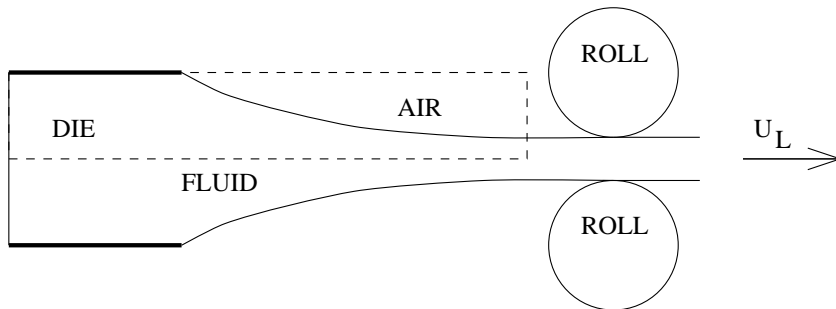


Figure 7: *Schematic view of film casting*

5 The Film Casting Problem

In this section, we briefly indicate how the developed methodology can be modified for the simulation of the film casting process. Figure 7 gives a schematic view of the problem. We define the draw ratio D_r :

$$D_r = \frac{U_L}{\bar{U}}, \quad (33)$$

with U_L the draw velocity and \bar{U} the average velocity of the flow at the die exit. As we will see, the stability of the interface (between fluid and air) depends on this draw ratio. The dashed line of figure 7 corresponds to the domain illustrated in figure 8.

As can be easily seen, the problem is similar to coextrusion with air

playing the role of the second polymer. Following Dhatt-Gao-Ben-Cheikh [9], air is considered as an incompressible fluid of very low viscosity. The

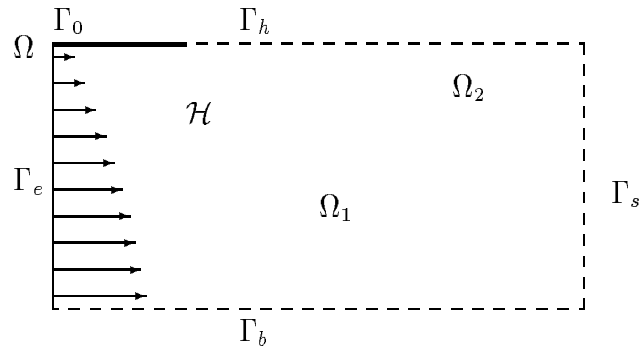


Figure 8: *Boundary conditions for film casting*

imposed boundary conditions are the following:

$$\begin{aligned}
 \vec{u} &= Q(u_0(y), 0) & \vec{x} \in \Gamma_e \\
 \vec{u} &= 0 & \vec{x} \in \Gamma_0 \\
 \boldsymbol{\sigma}_2 \cdot \vec{n} &= 0 & \vec{x} \in \Gamma_h \\
 u_2 = 0 &, \quad (\boldsymbol{\sigma}_1 \cdot \vec{n})_x = 0 & \vec{x} \in \Gamma_b \\
 \vec{u} &= (U_L, 0) & \vec{x} \in \Gamma_s
 \end{aligned} \tag{34}$$

At the die entry Γ_e , a half parabola with flow rate Q is imposed. A no-slip condition is imposed on Γ_0 while the flow (and thus the interface) is supposed fully developed with $\vec{u} = (U_L, 0)$ (the draw velocity) on Γ_s . Γ_b is a symmetry axis.

As in the coextrusion problem, a value of the pseudo-concentration is imposed at the entrance of the domain Γ_e . Its value will be transported in all the domain by the velocity field. We choose the following function:

$$S = 1 \quad \text{if } \vec{x} \in \Gamma_e. \tag{35}$$

Moreover, a velocity profile will be computed in the air (in Ω_2). Consequently, it is possible that $\vec{u} \cdot \vec{n} < 0$ on Γ_h and thus a boundary condition for S must be provided there when necessary. When this is the case, S is fixed to 0 on Γ_h .

Here again, the jump in the function will give the position of the interface between the fluid and the air.

5.1 The free-surface condition

The free surface condition

$$\boldsymbol{\sigma}_1 \cdot \vec{n} = 0, \quad \vec{x} \in \mathcal{H}. \quad (36)$$

is treated as a particular case of (17). Indeed, if we consider $\boldsymbol{\sigma}_2 \cdot \vec{n}$ in air:

$$\boldsymbol{\sigma}_2 \cdot \vec{n} = p_2 \vec{n} + \boldsymbol{\tau}_2 \cdot \vec{n} \quad (37)$$

But since the viscosity of air is supposed very small with respect to that of the polymer, $\boldsymbol{\tau}_2 \cdot \vec{n} \simeq 0$. Moreover, equation (1) gives

$$\nabla p_2 = 0 \quad (38)$$

which implies that $p_2 = \text{constant}$ in Ω_2 . From the condition $\boldsymbol{\sigma}_2 \cdot \vec{n} = 0$ on Γ_h , we conclude that $p_2 = 0$, thus $\boldsymbol{\sigma}_1 \cdot \vec{n} \simeq 0$

5.2 Solution algorithm

Both stationary and time-dependent solutions can be computed for this problem. For stationary solutions, the same algorithm (see section 4) as for the coextrusion problem is used.

For time-dependent solutions, the transport equation is given by (11) where the time derivative is discretized by the fully implicit Gear scheme (13). The Picard iterative scheme of section 4 has then to be used at each time step.

6 Numerical results

The results for the coextrusion and film casting problems are now presented. In both cases, the computations are started on a uniform mesh. When necessary, the mesh can be concentrated in some regions of the domain in a very simple manner. For example, in the coextrusion problem, a solution is computed on a uniform mesh and if one of the fluid layer is very small, the mesh is concentrated in the vicinity of that layer and a new computation is performed on the new mesh. This can be seen as a very primitive adaptive method. It is however easy to conceive a more sophisticated adaptive strategy

where one has to locate the discontinuity of the function S to decide where to refine the mesh. This strategy was not implemented in this work.

For the coextrusion problem, simulations with up to five different fluids are presented. For the film casting problem the main difficulty is to catch the movement of the interface in time. As we shall see, a Hopf bifurcation depending on the draw ratio and on the power index of the Carreau model occurs.

6.1 Coextrusion

The first example is the coextrusion of three polymers. This is a typical example where two polymers are coextruded and joined together by an adhesive. The adhesive is also a polymer but its width is very small compared to the two polymers. The rheological parameters for the different models are given in table 1. They correspond to a realistic coextrusion problem (see [22]).

The starting mesh is illustrated in figure 9 consisting of 30 elements in the y-direction by 40 elements in the x-direction. The dimension of the domain is 1 by 1.6667.

Starting with this uniform mesh, the interfaces were computed quite accurately but due to the coarse mesh, the adhesive layer fell within one element width. To improve the accuracy, the mesh was concentrated in the vicinity of the adhesive layer resulting in the mesh of Figure 10.

Figures 11 to 16 show the solutions obtained with the three models: Carreau, power law and Newtonian. Streamlines and interfaces positions are presented showing no fundamental difference between the three models.

A cross-section of the pseudo-concentration S at $x = 1.667$ (Figure 17) allows to compare the interface positions for the three models. The three plateaus gives the position of the different fluids. Only slight differences can be seen. Small oscillations are present but do not prevent an accurate estimation of the interface positions. As explained in Johnson [18], other methods would add numerical diffusion and the plateau corresponding to the adhesive would be lost.

Finally, a simulation with five polymers has been conducted. The uniform grid of Figure 9 and the Newtonian model were used. The constant viscosities are those given in Table 1. The polymers ABS-Adhefflon-PVDF-Adhefflon-ABS are ordered from bottom to top of the domain with respective flowrates

Models	Polymers	η_0 (Pa·s)	λ (s)	n	c	Flowrate
Carreau	ABS lower	8597	0.096	0.290	1	130
	Adheflon middle	7381	0.101	0.338	1	3.5
	PVDF upper	5224	0.093	0.443	1	10
Power law	ABS lower	45425	1	0.290	0	130
	Adheflon middle	33896	1	0.338	0	3.5
	PVDF upper	19601	1	0.443	0	10
Newton	ABS lower	8597	1	1	0	130
	Adheflon middle	7381	1	1	0	3.5
	PVDF upper	5224	1	1	0	10

Table 1: *Table of rheological parameters and flowrates (220°C)*

10-20-10-30-20 (adimensional units).

Figure 18 shows the pseudo-concentration at the entry ($x = 0$ and exit ($x = 1.667$) sections of the domain. This figure allows to compare between the initial and final position of the different fluids. Streamlines and interfaces positions are presented in the next two figures (19 and 20).

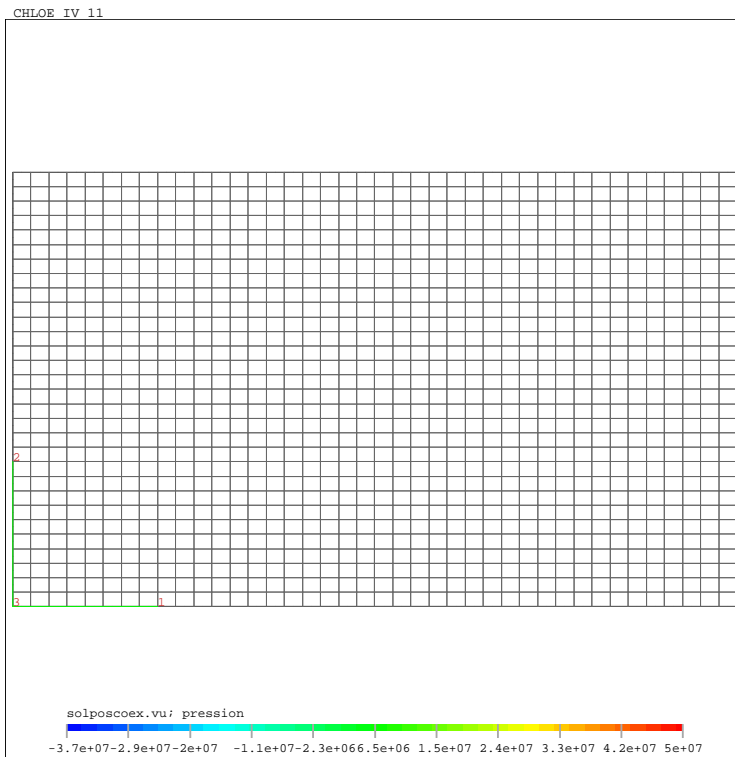


Figure 9: *Uniform mesh for coextrusion*

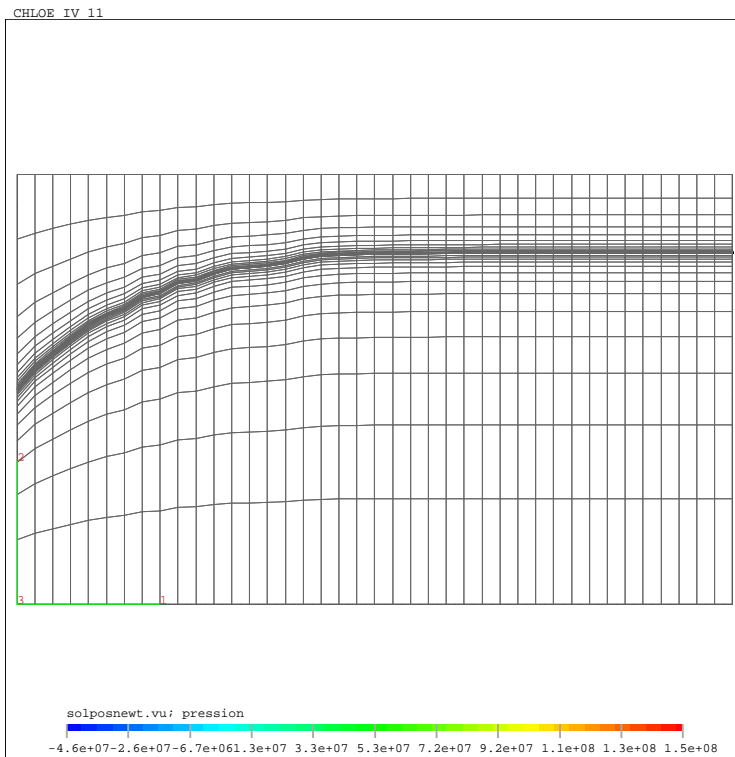


Figure 10: *Adapted mesh for coextrusion*

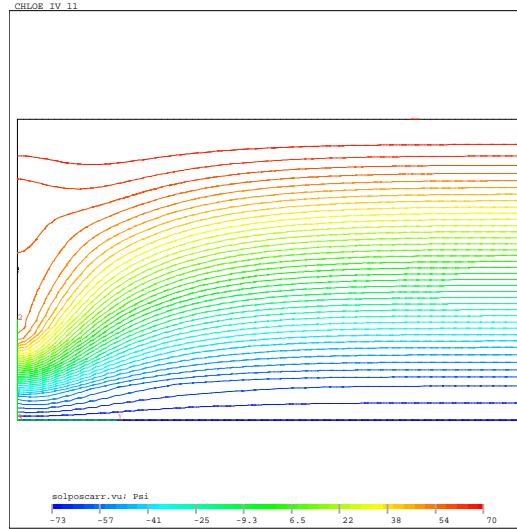


Figure 11: *Streamlines for Carreau fluids (3 polymers)*

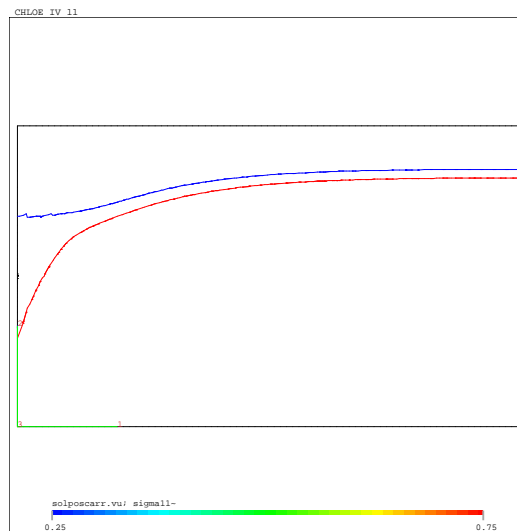


Figure 12: *Interface position for Carreau fluids (3 polymers)*

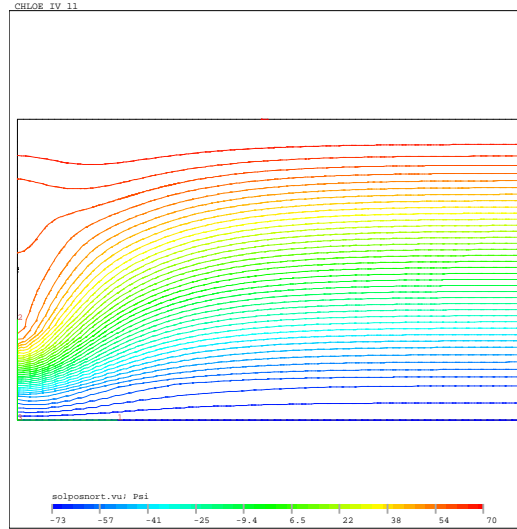


Figure 13: *Streamlines for power law fluids (3 polymers)*

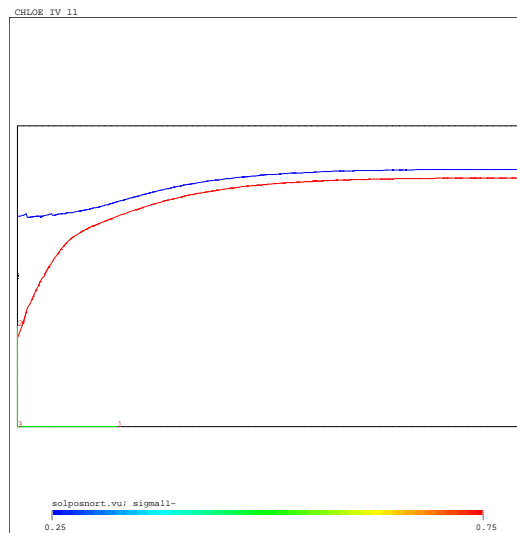


Figure 14: *Interface position for power law fluids (3 polymers)*

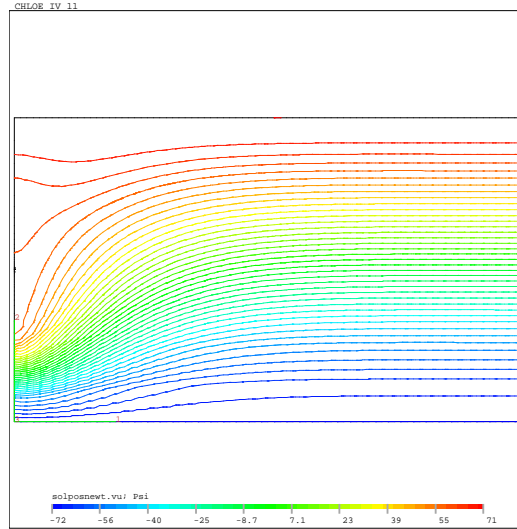


Figure 15: *Streamlines for Newtonian fluids (3 polymers)*

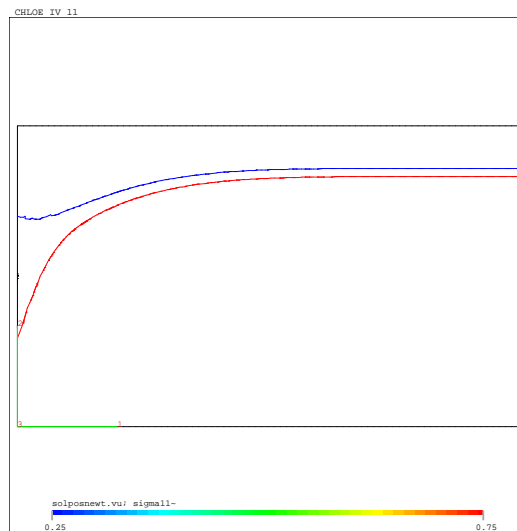


Figure 16: *Interface position for Newtonian fluids (3 polymers)*

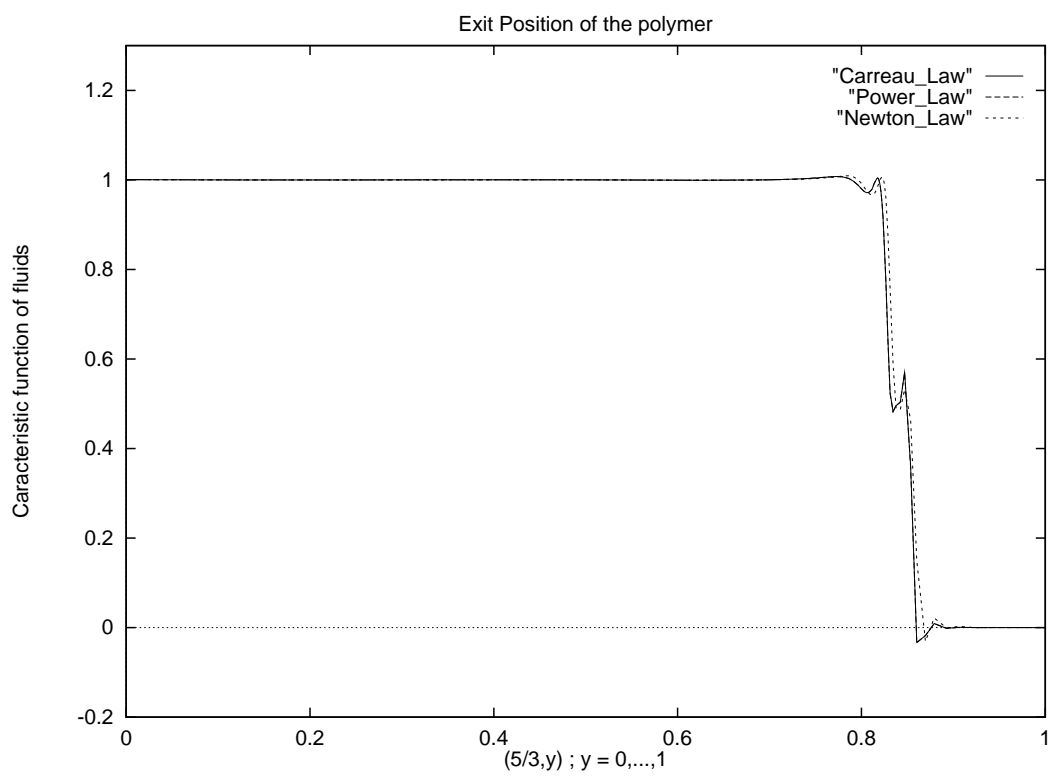


Figure 17: *Exit Section of the pseudo-concentration*

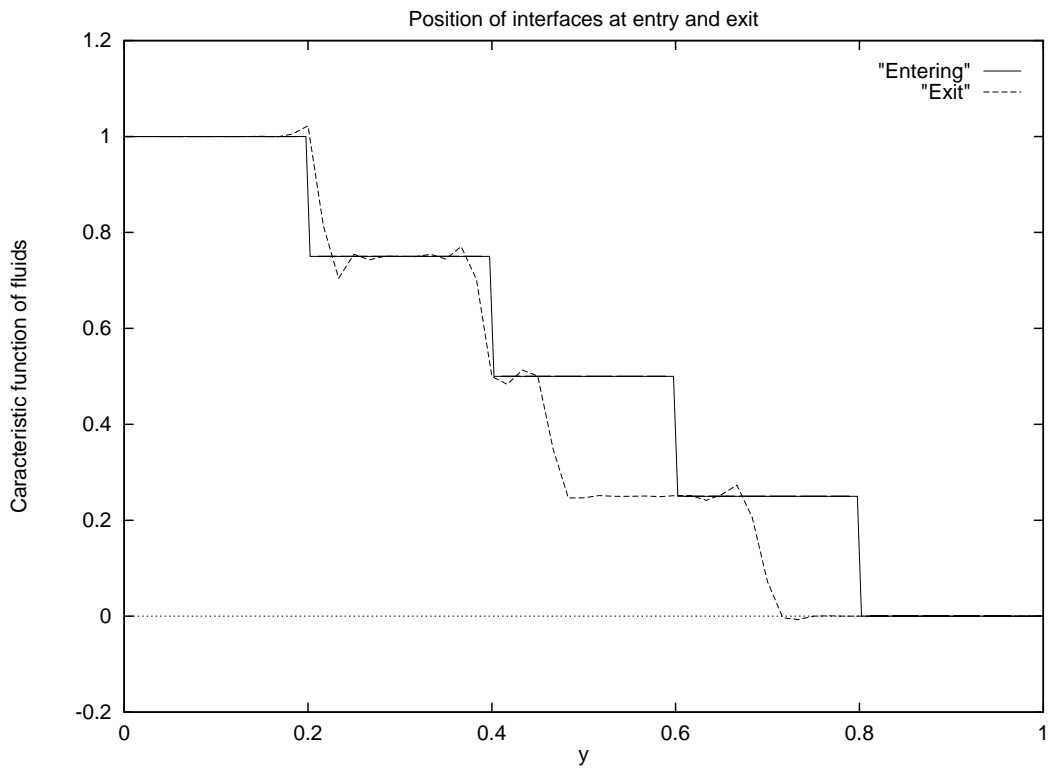


Figure 18: *Entry and Exit Section of the pseudo-concentration*

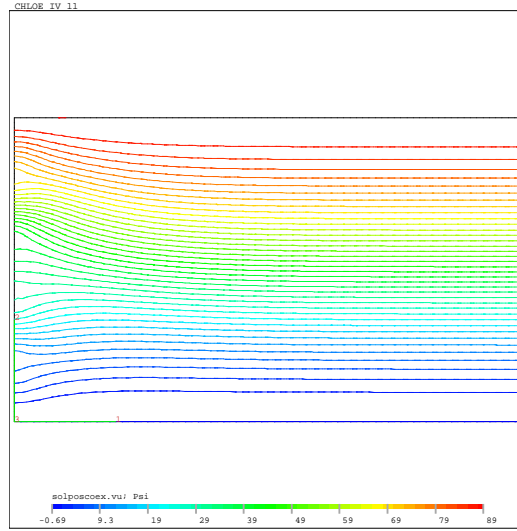


Figure 19: *Streamlines for Newtonian fluids (5 polymers)*

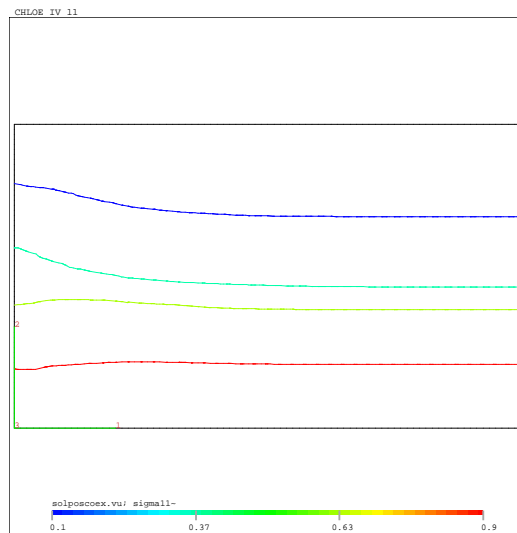


Figure 20: *Interface position for Newtonian fluids (5 polymers)*

6.2 Film casting

The solution strategy for the film casting problem is similar to the one used in the coextrusion problem. The dimension of the computational domain is 1 by 24 adimensional units (the die is 4 units long). In the following, the figures have been contracted by a factor 6 in the x-direction because it is barely possible to see anything when using the original dimension. Starting with a uniform mesh of 20 elements in the y-direction by 30 elements in the x-direction, a solution is computed for a Newtonian fluid and the mesh is concentrated in the vicinity of the free surface. A new computation is then performed. It is worth noticing that the solution on the uniform mesh is already acceptable but since our concern is the time-dependent case which results in small amplitude oscillations, we felt necessary to concentrate the mesh. This mesh is not very elegant, but it concentrates the mesh in the critical region.

The draw ratio is then slowly increased and stationary solutions are obtained up to $Dr = 20$. From now on, the mesh will be kept fixed. It is well known (see [8]) that this problem becomes time-dependent at a draw ratio around 21 in the Newtonian case ($n = 1$). Indeed, a Hopf bifurcation occurs and the free surface starts oscillating. The width of the film at the exit section varies with time as shown in figure 22. The next figures show the influence of the Carreau parameter n on the amplitude of the oscillations. Results are presented for $n = 0.75$, $n = 0.5$ and $n = 0.25$ (Fig. 23 to 25). A typical time-dependent free surface is illustrated in Fig. 26 to 31. The pulsating nature of the flow is easily seen by looking at the swelling of the free surface and the variation of the film width at the exit section.

It is clear that shear-thinning has a strong influence on the amplitude and a moderate one on the frequency as can be seen in Fig. 32 and Fig. 33. This is confirmed by the Fourier analysis of Fig. 34. As n decreases, the amplitude of the oscillations increases while the frequency decreases.

Finally, we have investigated the influence of shear-thinning on the critical draw ratio where the hopf bifurcation occurs. For $n = 0.25$, starting from the solution at $Dr = 21$, the draw ration was slowly decreased until the solution becomes stationary. At $Dr = 19$, the solution is still time-dependent as can be seen in Fig. 35. The solution is however stationary at $Dr = 18$ and the critical draw ratio is therefore somewhere around $Dr = 18.5$. It is therefore concluded that film casting of shear-thinning fluids will become unstable at

lower draw ratio.

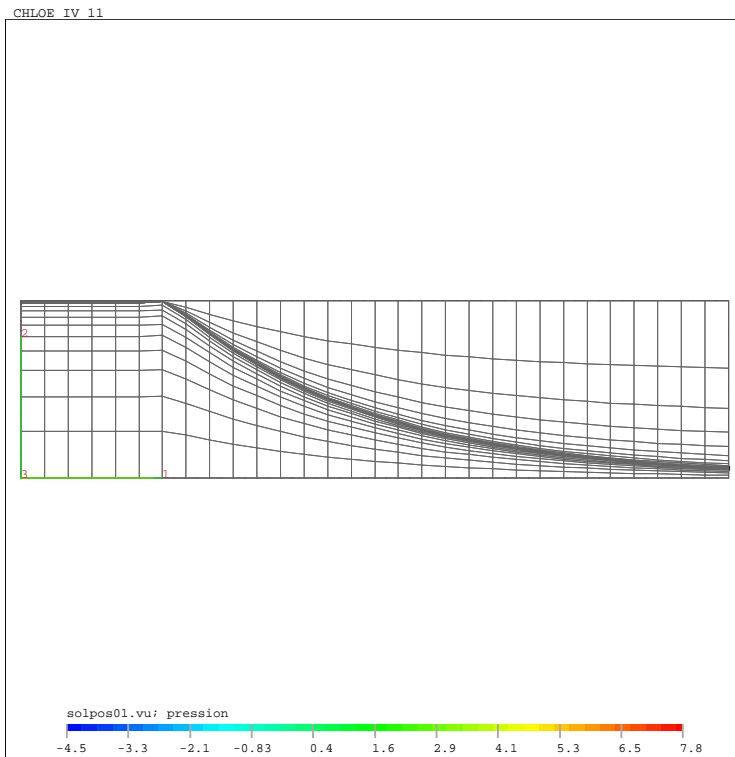


Figure 21: *Mesh for Film Casting*

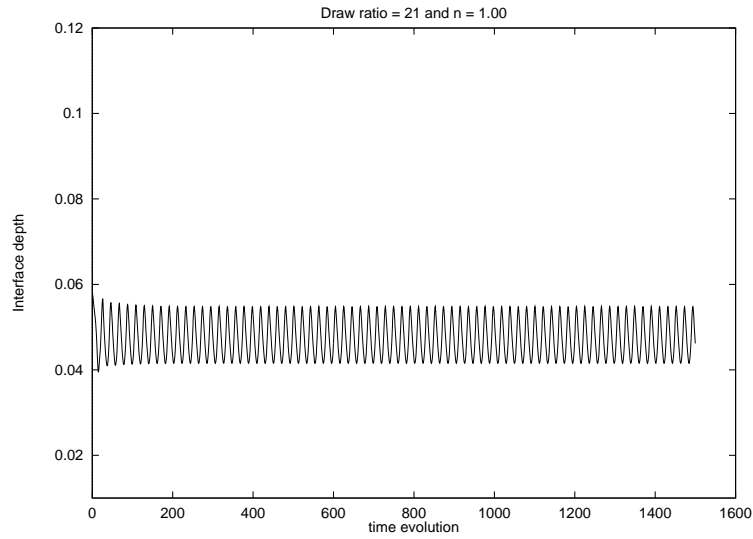


Figure 22: *Time-dependent film width, Draw ratio:21; n = 1.00*

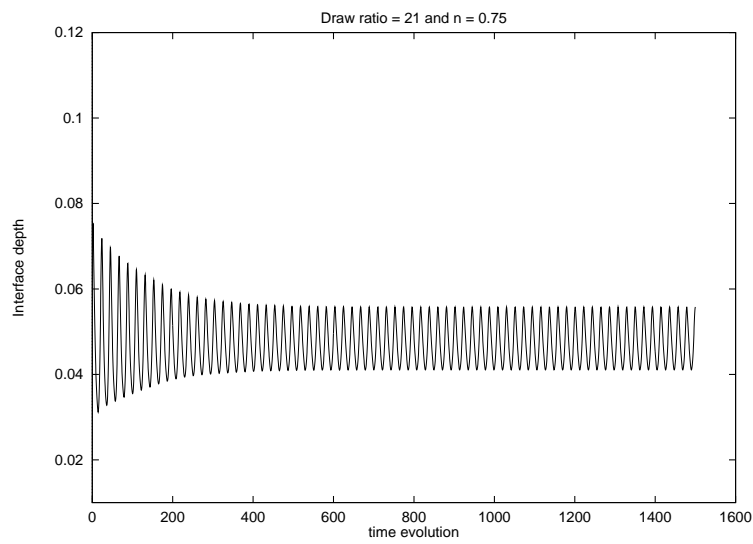


Figure 23: *Time-dependent film width, Draw ratio:21; n = 0.75*

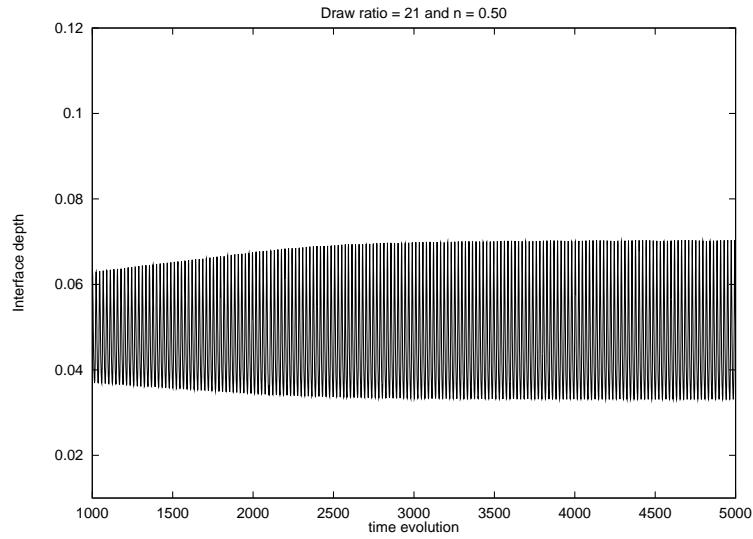


Figure 24: *Time-dependent film width, Draw ratio:21; n = 0.50*

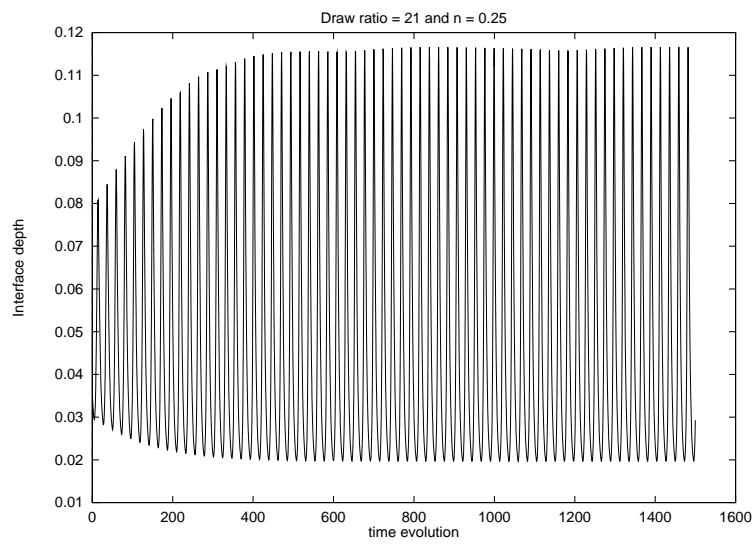


Figure 25: *Time-dependent film width, Draw ratio:21; n = 0.25*

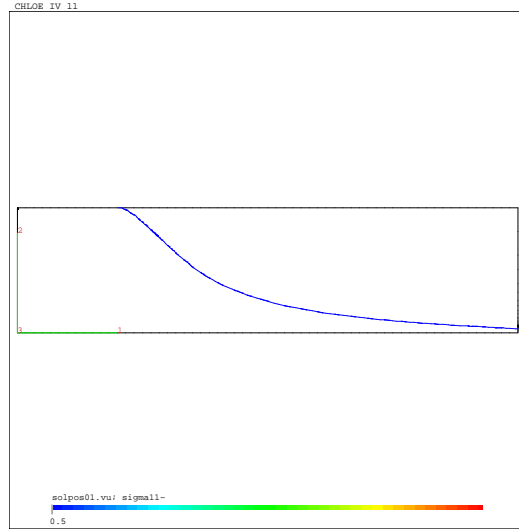


Figure 26: *Interface position at time T_0*

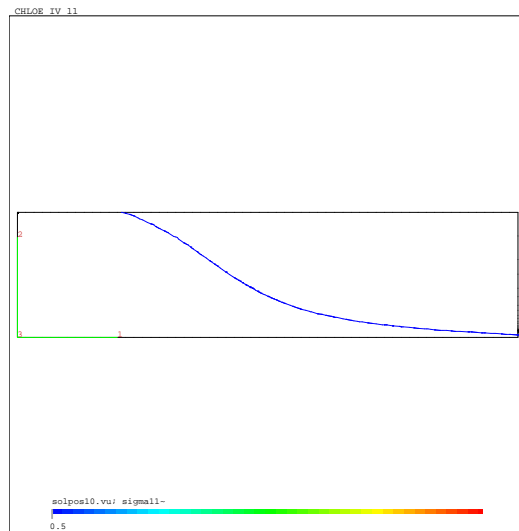


Figure 27: *Interface position at time $T_0 + 4,5$*

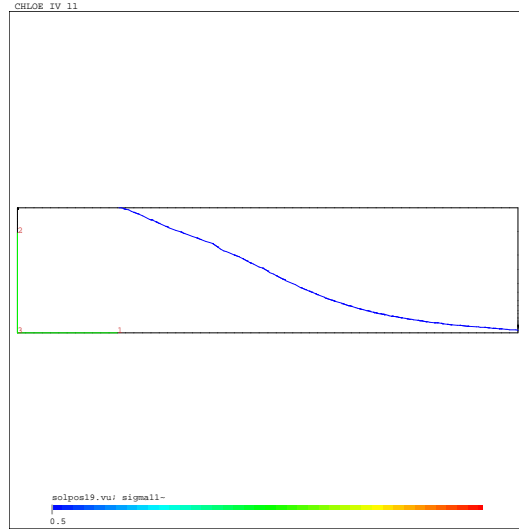


Figure 28: *Interface position at time $T_0 + 9,0$*

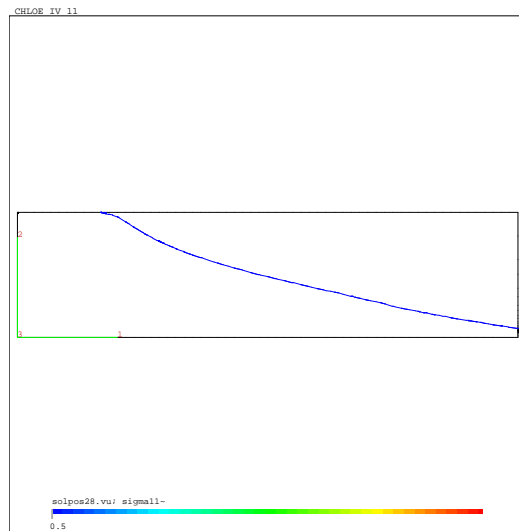


Figure 29: *Interface position at time $T_0 + 13,5$*

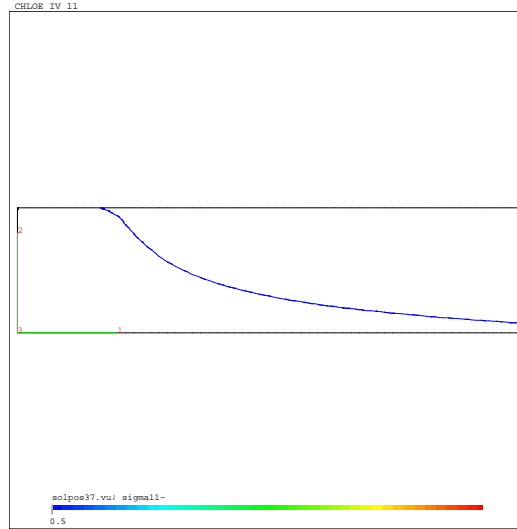


Figure 30: *Interface position at time $T_0 + 18$*

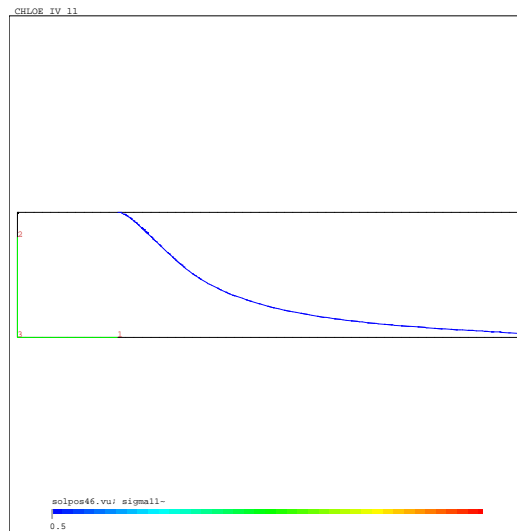


Figure 31: *Interface position at time $T_0 + 22,5$*

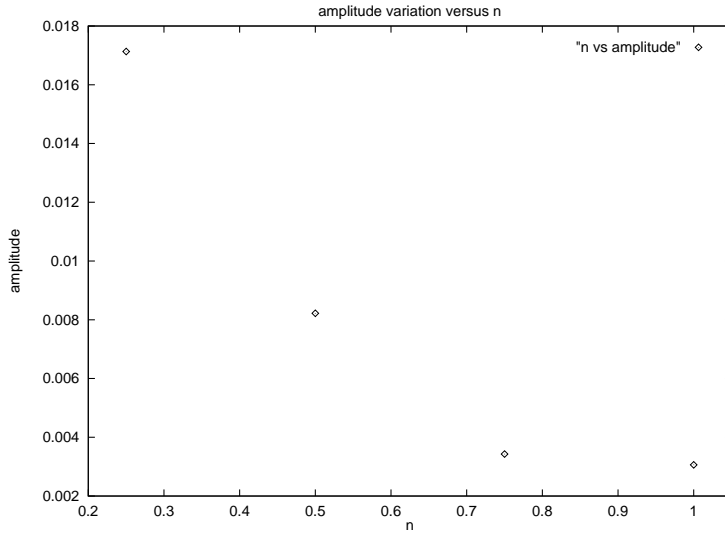


Figure 32: *Variation of amplitude with n*

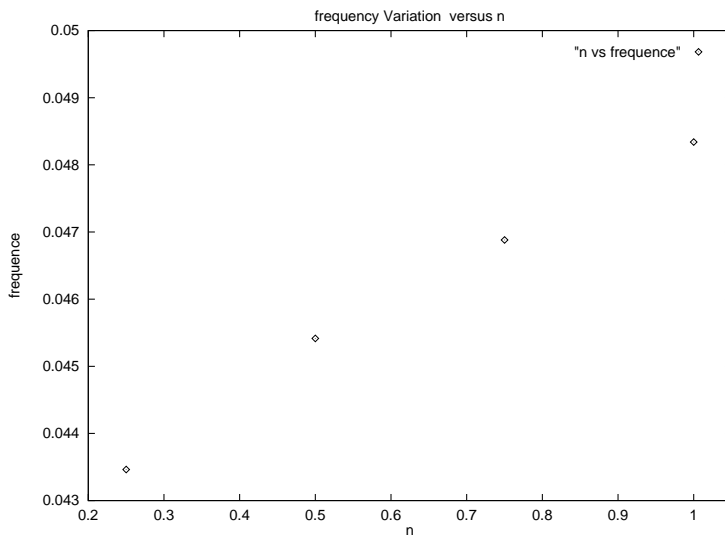


Figure 33: *Variation of frequency with n*

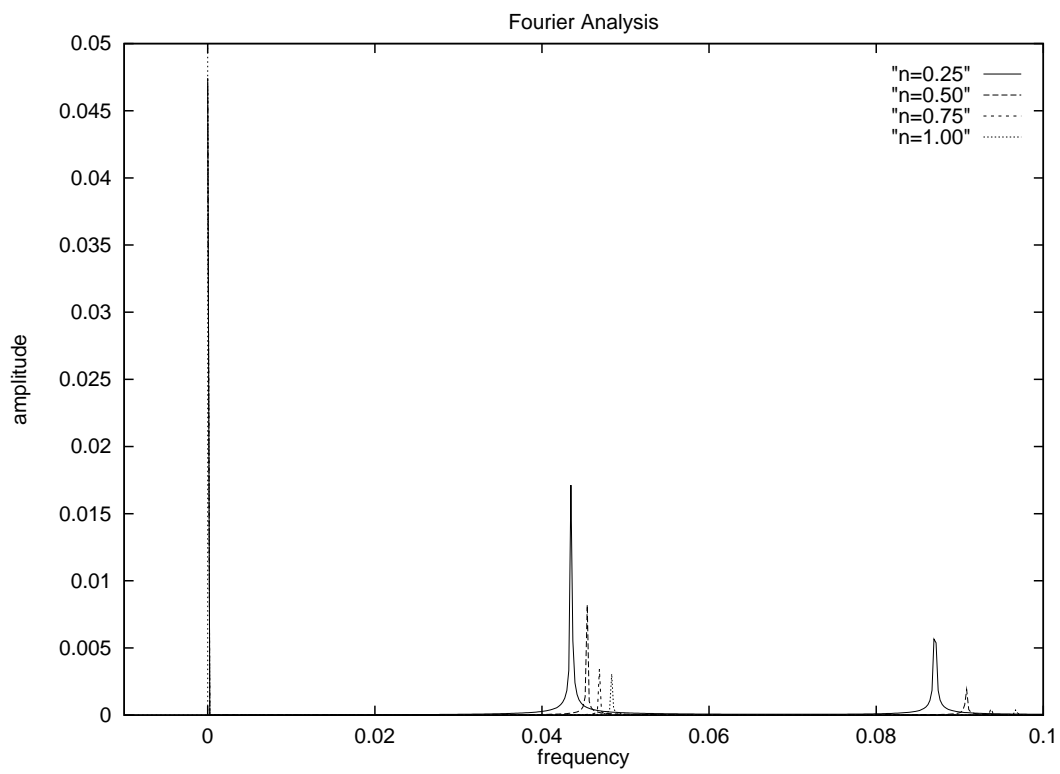


Figure 34: *Fourier analysis*

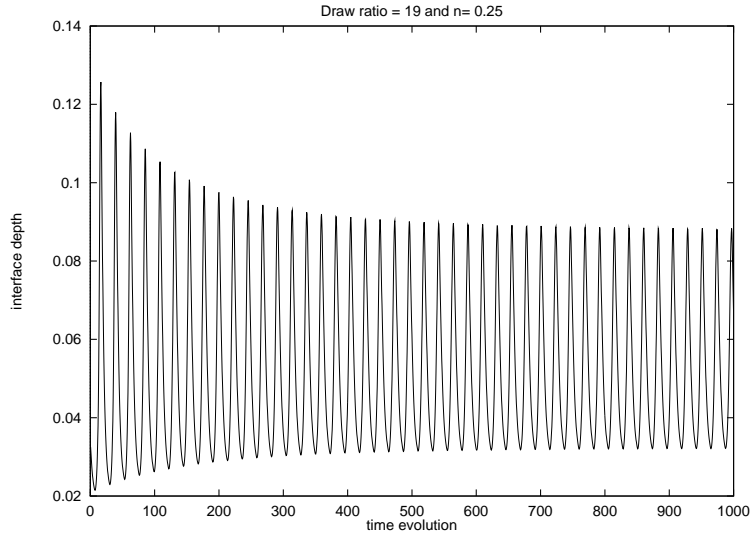


Figure 35: *Evolution to a time-dependent solution, Draw ratio:19*

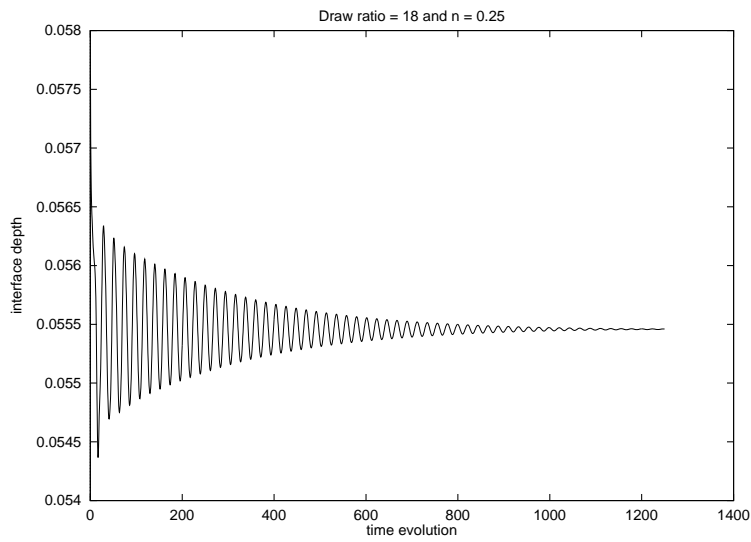


Figure 36: *Evolution to a stationary solution, Draw ratio:18*

7 Conclusion

This paper presents a numerical simulation of the coextrusion and film casting processes. The developed numerical method allows the computation of both stationary and time-dependent free surfaces in an efficient manner.

The results for film casting and coextrusion with up to five polymers show the flexibility of the algorithm. This opens the door to the investigation of the influence of the models and rheological parameters on different different polymer processes where free surfaces frequently occur.

A three-dimensional version of the present method is currently under development [11]. Our goal is to study encapsulation which is a purely three-dimensional phenomenon where the less viscous fluid tends to encapsulate (lubricate) the more viscous one. Linear stability for this problem has been studied in Joseph-Renardy-Renardy [19]. Preliminary results show that encapsulation can be captured by our method.

8 Acknowledgement

This work was partly supported by NSERC (Canada) and by FCAR (Québec).

References

- [1] J.F. AGASSANT, P.AVENAS, J.P. SERGENT, P. CARREAU, *Polymer Processing, Principles and Modeling*, Carl Hanser Verlag, pp.1-40.
- [2] J.F. AGASSANT, A. FORTIN, Y. DEMAY, *Prediction of Stationary Interfaces in Coextrusion Flows*, Polymer Engineering and Science, in press (1993)
- [3] P.BARQ, J.M. HAUDIN, J.F. AGASSANT, H.ROTH et P. BOURGIN, *Instability Phenomena in Film Casting Process*, International Polymer Processing, V (1990) 4, pp.264-271.
- [4] R.B BIRD, R.C. ARMSTRONG, O. HASSAGER, *Dynamics of Polymer Liquids*, Volume 1, Fluid Mechanics, John Wiley and Sons, (1977), 470 pages.
- [5] BREZZI, M.FORTIN, *Mixed and Hybrid Finite Element Methods*, Springer-Verlag, (1990).
- [6] P.CARRIER, *Calcul des surfaces libres de procédés de mise en forme des polymères*, Mémoire présenté à l'École Polytechnique de Montréal, Août 1993.
- [7] M.J. CROCHET, V. DELVAUX, J.M. MARCHAL, *Numerical Prediction of Viscoelastic Extrudate Swell*, NUMIFORM 89, Thompson et al. (eds), Balkema, Rotterdam, pp.17-22, (1989)
- [8] Y. DEMAY, J.F. AGASSANT, *Experimental Study of the Draw Resonance in Fiber Spinning*, Journal of Non-Newtonian Fluid Mechanics, 18, (1985), pp.187-198.
- [9] G. DHATT, D.M. GAO, A. BEN CHEIKH, *A Finite Element Simulation of Metal Flow in Moulds*, Int. J. Num. Meth. Engrg. vol. 30, (1990), pp.821-831.

- [10] A. FORTIN, Y. DEMAY, J.F. AGASSANT, *Computation of Stationary Interface Between Generalized Newtonian Fluids*, Revue Européenne des Éléments Finis, Vol. 1, No. 2, (1992), pp. 181-196.
- [11] A. FORTIN, J. TEIXEIRA, Y. DEMAY, J.F. AGASSANT, *in preparation*.
- [12] A. FORTIN, M. FORTIN, J.J. GERVAIS, *A Numerical Simulation of the Transition to Turbulence in a Two-Dimensional Flow*, J. of Comp. Physics, 70(2), pp.295-310, (1987).
- [13] A. FORTIN, A. ZINE, J.F. AGASSANT, *Computing Viscoelastic Fluid Flow problems at Low Cost* J. Non-Newt. Fluid Mech., 45(2), pp.209-229, (1992).
- [14] M. FORTIN, A. FORTIN, *A Generalization of Uzawa's Algorithm for the Solution of the Navier-Stokes Equations*, Communications in Applied Numerical Methods, Vol. 1, (1985), pp.205-208,
- [15] M. FORTIN, A. FORTIN, *Experiments with Several Elements for Viscous Incompressible Flows*, Int. Journal For Numerical Methods in Fluids, Vol. 5, (1985), pp.911-928.
- [16] M. FORTIN, R. GLOWINSKI, *Résolution numérique de problèmes aux limites par des méthodes de lagrangien augmenté.*, Coll. mathématiques, série mathématiques pures et appliquées, Département de mathématiques, Université Laval.
- [17] C.W. HIRT, B.D. NICHOLS, *Volume of Fluid (VOF) method for the dynamics of free boundaries*, J. Comput. Physics, vol. 39, (1981), pp.201-225.
- [18] C. JOHNSON, *Numerical Solution of Partial Differential Equations by the Finite Element Method*, Cambridge University Press, (1990), 278p.
- [19] D.D. JOSEPH, M. RENARDY, Y. RENARDY, *Instability of the flow of two immiscible liquids with different viscosities in a pipe*, J. Fluid Mech., vol. 141, pp. 309-317, (1984).

- [20] J.M. OTTINO, *Cambridge Texts in Applied Mathematics*, Cambridge University Press, (1989), 364 pages.
- [21] D.PELLETIER, A.ZAKI, A.FORTIN, *Adaptive Remeshing for Hyperbolic Transport Problems*, submitted to the J. of Fluid Dynamics.
- [22] S. PUISSANT, *Etude numérique et expérimentale de la coextrusion des polymères dans une filière plate*, Thèse présentée à l'Ecole Nationale Supérieure des mines de Paris, (1992).
- [23] S.F. SHEN, *Grappings with the Simulation of Non-Newtonian Flows in Polymer Processing*, Int. J. Num. Meth. in Engrg. , 34, 701-723, (1992).
- [24] E. THOMPSON, *Use of Pseudo-Concentrations to Follow Creeping Viscous Flows During Transient Analysis*, Int. J. Numer. Meth. Fluids, vol. 6, (1986), pp.749-761.
- [25] E. THOMPSON, R.E. SMELSER, *Transient Analysis of Forging Operations by the Pseudo-Concentration Method*, Int. J. Numer. Meth. Engrg., vol. 25, (1988), pp.177-189.
- [26] A. ZAKI, *Simulation numérique de problèmes de convection sur des maillages adaptatifs non-structurés du type h-p*, Thèse présentée à l'Ecole Polytechnique de Montréal, (1993).